CONF-900789--2

EMBRITTLEMENT OF THE SHIPPINGPORT REACTOR NEUTRON SHIELD TANK*

O. K. Chopra, S. T. Rosinski†, and W. J. Shack

Materials and Components Technology Division
ARGONNE NATIONAL LABORATORY
9700 South Cass Avenue, Argonne, IL 60439

† SANDIA NATIONAL LABORATORIES
P. O. Box 5800, Albuquerque, NM 87185

CONF-900789--2

DE90 010464

January 1990

DISCLAIMER

To be presented at the *Symposium on Degradation of Ferritic, Austenitic and Duplex Stainless Alloys in Nuclear Service*, the 1990 ASME Pressure Vessels and Piping Conference, Nashville, TN, June 17-21, 1990.

*Work supported by the Office of Nuclear Regulatory Research, U. S. Nuclear Regulatory Commission.

EMBRITTLEMENT OF THE SHIPPINGPORT REACTOR NEUTRON SHIELD TANK*

O. K. Chopra, S. T. Rosinski†, and W. J. Shack

Materials and Components Technology Division

ARGONNE NATIONAL LABORATORY

9700 South Cass Avenue, Argonne, IL 60439

† SANDIA NATIONAL LABORATORIES

P. O. Box 5800, Albuquerque, NM 87185

Abstract

The irradiation embrittlement of the Shippingport neutron shield tank material (A212 Grade B steel) has been characterized. Irradiation increases the Charpy transition temperature (CTT) by 23 - 28°C (41 - 50°F) and decreases the upper shelf energy. The shift in CTT is not as severe as that observed in the HFIR surveillance specimens. However, the actual value of CTT is higher than that for the HFIR data and the toughness at service temperature is low. The increase in yield stress is 51 MPa (7.4 ksi), which is comparable to the HFIR data. The results also indicate that the material is weaker in the TL orientation than LT orientation. Some effects of the location across the thickness of the wall are also observed; CTT is slightly greater for the specimens from the inner region of the wall. The data agree well with results from high-flux test reactors. Annealing studies indicate complete recovery of embrittlement after a 2-h anneal at 400°C. Although the weld metal is

significantly tougher than the base metal, the shifts in CTT are comparable. The weld metal shows a strong affect of location across the thickness of the wall; only the inner regions of the weld show embrittlement.

1. Introduction

Surveillance specimens from the high flux isotope reactor (HFIR) at Oak Ridge National Laboratory showed a very high degree of embrittlement compared with data obtained on similar materials in materials testing reactors .[1-3] One explanation of the difference between the HFIR data and the test reactor data is that, for a given irradiation level, embrittlement is greater at lower flux. Since current NRC guidelines for the assessment of the embrittlement of the pressure vessel support structures of commercial light water reactors do not consider flux, the HFIR results raise the possibility that they may not be sufficiently conservative.

To help resolve this issue, a program was initiated to characterize the irradiation embrittlement of the neutron shield tank (NST) from the decommissioned Shippingport reactor. The Shippingport NST, which operated at 55°C (130°F), was fabricated from rolled A212 grade B firebox steel similar to that used for the HFIR vessel. The inner wall of the NST was exposed to a total maximum fluence of ~6 x 10^{17} n/cm^2 (E>1 MeV) over a life of 9.25 effective–full–power years. This corresponds to a fast flux of 2.1 x 10^9 n/cm^2·s. In comparison the HFIR surveillance specimens were exposed at the inner surface of the

pressure vessel at a temperature of 50°C (122°F) over a period of ~17 effective-full-power years; the flux of fast neutrons was ~2 x 10^{8} n/cm^2 s.[1]

2. Material Characterization

The effort to obtain samples from the NST was sponsored jointly by the NRC and the DOE Plant Life Extension Program (PLEX) at Sandia National Laboratories (SNL). The actual sampling was performed by personnel from Battelle Pacific Northwest Laboratory. The details of the sampling are presented elsewhere.[4,5] Eight ~155 mm (~6 in) disc samples of the base metal and three weld samples were obtained from the inner wall, along with the corresponding samples from the outer wall. The layouts for the sample locations from the inner and outer walls are shown in Fig. 1. The inner wall is constructed from four plates ~25.4-mm (1 in) thick, welded after assembly. The two lower plates were joined by vertical full-penetration welds located along the azimuthal positions 0 and 180° (north and south reference axes of the NST) and the lower plates were welded along the azimuthal positions 135 and 315°. These two assemblies were joined by a mid-height horizontal full-penetration weld. Thus, specimen locations 13, 14, and 15 contain vertical welds; the other locations represent the base metal from the four plates. The total fluence varied among the various locations; the maximum vertical fluence occurred at an elevation of 211.07 m (692.5 ft), whereas the maximum azimuthal fluence occurred at the 20 and 200° positions. The estimated fluence was ~6 x 10^{17} n/cm^2 (E>1 MeV) for locations 3 and 9; ~4 x 10^{17} n/cm^2 for locations 2 and 8; ~3 x 10^{17} n/cm^2 for locations 14 and 15; and ~2 x 10^{17} n/cm^2 for location 13.[6]

The outer wall was constructed from two plates joined together by vertical welds at azimuthal positions 0 and 180°. All samples from the outer wall represent base metal from the two plates. A weld sample was obtained from the outer wall at location 1. No effect of irradiation is expected at the extremely low levels of irradiation for the outer wall; therefore, the outer wall samples were used to determine the unirradiated baseline data. Additional samples from the essentially unirradiated lower portion of the NST outer wall, viz., locations L1 - L4, were also procured for obtaining baseline material properties.

Metallurgical characterization and chemical analyses of samples taken from each of the plates strongly suggest that both the inner and outer walls of the NST were fabricated from a single heat. Typical chemical analyses for the plate and weld metal are given in Table 1. Metallographic examination of the NST material indicates that the rolling direction is horizontal. Micrographs of the grain structure along the rolling and transverse directions are shown in Fig. 2. The surfaces shown in the micrographs are designated by the direction normal to that surface. The transverse section shows some elongated grains and all the inclusions are elongated in the rolling direction. The inclusions in the rolling section are globular or flat.

There are significant variations in hardness across the thickness of the NST wall. In general, the center of the plate is softer than the near-surface regions. A typical through-wall hardness profile (Rockwell B) for the outer wall is shown in Fig. 3a. (The depth is measured from the inner surface of the plate, i. e., the surface towards the reactor core.) The hardness varies between R_B 73 and 83, and values of the inner and outer regions of the

wall are 5 to 10% higher than those of the wall center. However, no measurable change in grain size was observed across the thickness of the wall; the average through-wall grain size was ~12 μm. Although irradiation increases the hardness of the material, the V-shape profile is maintained at most locations of the inner wall. The hardness profile for location 9 of the NST inner wall is shown in Fig. 3b. Material from a few locations of the inner and outer walls showed little or no variation in hardness across the wall thickness.

3. Irradiation Embrittlement

The irradiation embrittlement has been characterized by Charpy impact and tensile tests. Specimens were obtained in the LT and TL orientations* from three regions, i.e., inner, center, and outer 10-mm-wide regions, across the thickness of the NST wall. A typical layout for the base metal specimens from the inner and outer walls is shown in Fig. 4. Material from the outer wall, which was protected by ~0.9 m (3 ft) of water and hence had a six-order-of-magnitude lower fluence than the inner wall, was used to obtain baseline data for unirradiated material.

Charpy impact tests were conducted on standard Charpy V-notch specimens machined according to ASTM specification E 23. A Dynatup Model 8000A drop weight impact machine with an instrumented tup and data readout system was used for the tests. Tensile

---

* The first digit designates the direction normal to the plane of the crack; the second digit represents the direction of crack propagation. L = longitudinal or rolling direction and T = transverse direction.

tests were performed on dog bone specimens, with a cross section of 4 x 5 mm and a gauge length of 20 mm. The tests were conducted at an initial strain rate of 4×10^{-4} s^{-1}.

3.1 Base Metal

3.1.1 Charpy Impact Energy

Charpy transition curves for the LT and TL specimens from different regions of the NST outer and inner walls are shown in Figs. 5-7. The Charpy data were fitted with a hyperbolic tangent function of the form

$$KCV = K_O + B\{1 + \tanh [(T-C)/D]\}, \qquad (1)$$

where Ko is the lower-shelf energy, T is the test temperature, B is half the distance between upper- and lower-shelf energy, C is the mid-shelf Charpy transition temperature (CTT) in °C, and D is the half-width of the transition region. The values of the constant in Eq. (1) as well as the values of CTT at 20.3-J (15 ft·lb) level and upper shelf energy (USE) for the various samples are given in Table 2. The best-fit curves are shown in the figures.

The results for the outer wall, Fig. 5, indicate little or no variation in the transition curves with vertical and azimuthal positions. However, the TL orientation is weaker than the LT orientation. The CTT and USE, respectively, are 16°C (61°F) and 102 J/cm^2 (~60 ft·lb) for LT specimens and 20°C (68°F) and 67 J/cm^2 (~40 ft·lb) for TL specimens. The differences in impact strength are attributed primarily to differences in the

distribution of inclusions along the crack plane. The plane of the crack for TL orientation, i.e., transverse section shown in Fig. 2, contains elongated inclusions.

The results also indicate some effect of position through the thickness of the wall; impact energies for specimens from the inner and outer regions of the wall are comparable, whereas those for the center specimens are slightly higher. The CTT and USE for the center specimens are, respectively, 9°C (48°F) and 103 J/cm^2 (~61 ft·lb) for LT orientation and 2°C (36°F) and 74 J/cm^2 (~44 ft·lb) for TL orientation. This correlates with the differences in the hardness of the material. The hardness of the center region is in the range of R_B 73 - 75 (132 - 142 DPH) and R_B 78 - 84 (144 - 162 DPH) for the inner or outer regions.

Charpy impact energies for essentially unirradiated material from location L4 of the outer wall, shown in Fig. 6, are in good agreement with the data for material from other locations. The results indicate that the Charpy transition curves for outer-wall material represent baseline data for unirradiated material. As discussed in section 2, the hardness of the center of the wall varies significantly for different locations. The data for the center specimens may not be representative of all locations. Therefore, results for only the inner and outer regions of the wall are used to characterize irradiation embrittlement.

The transition curves for the LT and TL specimens from different locations of the NST inner wall, are shown in Fig. 7. The irradiated inner wall specimens show a higher CTT and lower USE relative to those from the unirradiated outer wall. The transition curves are

almost independent of vertical position, which suggests that a factor of two in the variation of fluence has relatively little effect. For example, the impact energies for specimens from locations 2 and 8 (~4 x 10^{17} n/cm^2 fluence) are comparable to those for specimens from locations 3 and 9 (~6 x 10^{17} n/cm^2 fluence). For LT specimens, some differences are observed for those from the inner and outer regions of the wall; the shift in CTT is slightly greater for the inner region. The values of CTT are 39°C (102°F) for the outer region and 44°C (111°F) for the inner region, a shift of ~23 and 28°C (~41 and 50°F) for the outer and inner regions, respectively. The USE can not be established from the data in Figs. 7a and 7b. However, the specimens tested at 55°C show 100% shear fracture; thus, the impact energy for these specimens, i.e., an average value of ~77 J/cm^2 (45 ft·lb), is representative of USE.

The shift in CTT of the inner-wall TL specimens, Fig. 7c, is also 23°C (41°F), similar to that for the LT specimens. However, the USE is lower, 52 J/cm^2 (31 ft·lb). The effect of position through the thickness of the wall is minimal for the these specimens. The impact energies for the center specimens are comparable to those for specimens from the inner and outer region. Variation in through-wall hardness is also minimal for locations 14 and 15 of the inner wall.

3.1.2 Tensile Properties

Tensile tests were conducted at room temperature and at 55°C (131°F) on LT specimens from several locations of the NST inner and outer walls and three regions across

the thickness of the wall. The results indicate little or no variation with vertical and azimuthal positions, i.e., tensile strength for locations 2 and 8 (~4 x 10^{17} n/cm^2 fluence) is comparable to that for locations 3 and 9 (~6 x 10^{17} n/cm^2 fluence). Tensile strength for the inner wall is higher relative to the outer wall. Hardness influences the tensile properties at both test temperatures, i.e., the yield and ultimate stresses for the specimen from the center of the wall are always lower than those for the specimens from inner or outer regions. Average tensile properties for outer and inner walls are given in Table 3. The increases in yield and ultimate stress are, respectively, ~51 and 20 MPa (~7.4 and 2.9 ksi) at room temperature and ~38 and 18 MPa (~5.5 and 2.6 ksi) at 55°C. The increase in yield and ultimate stress due to irradiation, is the same for specimens from the center and from the inner or outer regions of the walls.

The tensile properties of the NST material were also estimated from the Charpy impact data. The yield stress is estimated from the expression

$$\sigma_y = AP_yB/Wb^2, \qquad (2)$$

taken from Ref. 7, where P_y is the yield load obtained from the load-time traces of the instrumented Charpy tests, W is the specimen width, B is the specimen thickness, b is the uncracked ligament, and A is a constant. The constant A was obtained by comparing the tensile and Charpy data for LT specimens tested at room temperature and at 55°C. The best value of the constant was 1.73. The yield loads and the estimated yield stresses for the outer and inner walls are shown in Fig. 8. The measured yield stresses are compared with the estimated values. The results show the expected decrease in yield stress with an

increase in test temperature. In the lower-shelf temperature regime, cleavage occurs before general yielding; therefore, the yield loads are very low. For the Charpy impact tests, cleavage fracture occurs when the yield loads are ~13 kN. Irradiation increases the yield stress at all test temperatures and, therefore, the CTT shifts to higher temperatures. Irradiation hardening is greater at room temperature than at higher temperatures.

3.1.3 Recovery Annealing

Annealing studies were conducted on material from the NST inner and outer walls to study the recovery behavior of embrittled material. Specimens were annealed at 400°C for up to 154 h and the annealing behavior was characterized by hardness measurements. The results indicate that the hardness of irradiated material from the inner wall decreases after annealing, whereas the hardness of the outer-wall material increases. Annealing for 1 h at 400°C (752°F) was sufficient for recovery; only a very slight increase in hardness of both the inner- and outer-wall materials occurs after annealing for longer times. The changes in hardness of material from inner and outer walls, shown in Fig. 9, reflect the differences in the fluence and flux levels of the different locations, i.e., the decrease for locations 3 and 9 is greater than for location 8.

Charpy impact data for TL specimens from the NST inner and outer walls, annealed for 2 h at 400°C, are shown in Fig. 10. The results indicate a complete recovery from irradiation embrittlement, i.e., the transition curve of the annealed specimens from the inner wall is identical to that of the outer wall. Annealing has little or no effect on the

transition curve of the outer wall. These results confirm that the data for outer-wall material represents baseline data for unirradiated material

3.2 Weld Metal

Weld samples were obtained at one position on the outer wall (location 1) and three positions on the inner wall, i.e., locations 14 and 15 with ~3 x 10^{17} n/cm^2 fluence and location 13 with ~2 x 10^{17} n/cm^2 fluence. All the welds were transverse to the plate rolling direction. Charpy impact test specimens were machined perpendicular to the weld and from the inner and outer regions across the thickness of the plate. The chemical composition of weld metals from different locations indicates only minor variations in silicon and copper content, Table 1. Annealing studies were also conducted on the weld specimens to obtain baseline data and to help characterize the irradiation embrittlement of the welds.

Charpy transition curves for the weld metal specimens, with or without recovery annealing for 2 h at 400°C, are shown in Figs. 11 and 12. The best-fit curves to Eq. (1) are also shown in the figures. The impact strength of the outer-wall weld is significantly higher than that of the base metal, Fig. 11. The 41-J (30 ft-lb) CTT and USE of the weld are -7°C (28°F) and 184 J/cm^2 (109 ft-lb), respectively. Location through the thickness of the weld, i.e., inner and outer regions, has no effect on the transition curve. Annealing has little effect on the specimens from inner region of the outer-wall weld, whereas, impact energy of annealed specimens from the outer region is significantly increased after

annealing. The increase in impact energy can be attributed to microstructural changes due to thermal aging. The results suggest that the Charpy data for the annealed specimens may reflect recovery of irradiation embrittlement as well as from thermal aging.

The inner-wall specimens show a strong affect of location across the thickness of the wall. The transition curves for the inner region of the inner–wall welds are shown in Figs. 8c and 8d. The 41-J (30 ft·lb) CTT is 14°C (57°F) for the weld at location 14 and 13°C (55°F) for welds at locations 13 and 15, i.e., a shift of 21 and 20°C (38 and 36°F), respectively, relative to the data for the outer-wall weld. Weld specimens from the outer region show no irradiation embrittlement relative to the outer-wall weld, Figs. 12c and 12d. Charpy transition curve for the outer-region specimens from location 14 is comparable, while that from locations 13 and 15 is slightly higher than that for the outer-wall weld. The results for annealed specimens from inner region of location 14 indicate recovery from irradiation embrittlement, i.e., the impact energies compare well with those for outer-wall weld. However, weld specimens from inner and outer regions of location 15 and outer region of location 14 show a large increase in impact energy after annealing. These results are similar to outer-region weld from outer wall and primarily reflect thermal aging affects caused by microstructural instabilities. The annealing data, therefore, can not be used to characterize irradiation embrittlement.

4. Discussion

Charpy impact and tensile data for the Shippingport NST indicate that the shift in CTT is not as severe as would be expected on the basis of the changes seen in HFIR surveillance samples. In Fig. 13, Charpy transition curves for the outer and inner walls of the NST are compared with the results for unirradiated and irradiated HFIR surveillance samples. Although the shift is smaller, the actual CTT of the NST material is significantly higher than that of the HFIR material. The impact energy of the NST inner wall is very low, ~40 J/cm^2 (24 ft·lb), at the service temperature of 55°C (130°F).

Except for minor differences in copper and nickel content, the chemical composition of the two materials is comparable. The concentrations of copper and nickel are 0.15 and 0.20 wt.%, respectively, for HFIR material and 0.05 and 0.04 wt.% for NST. Although the HFIR material is tougher than the NST material, the tensile strength of the HFIR material is greater than that of the NST material. The yield strength and hardness, respectively, are 355 ± 11 MPa (~51 ± 2 ksi) and 170 DPH for the HFIR material[2] and 305 ± 19 MPa (44 ± 3 ksi) and 159 DPH for NST. The difference in the transition curves of the two unirradiated materials is most likely due to microstructural factors, such as the amount and distribution of inclusions.

When the shifts in CTT of the NST material are compared with the results obtained from the HFIR material irradiated in the ORR and other A212B steels irradiated in high-flux test reactors, Fig. 14, the results from the Shippingport NST are consistent with the

test reactor data. Estimates of neutron fluence[6] and activation measurements[8] indicate that the fluence decreases by a factor of 2 to 3 across the thickness of the NST inner wall. The fluence for the outer-region specimens were estimated to be a factor of ~1.5 lower than that for the inner-region specimens. The results for the NST material also agree very well with correlations for the shift in CTT, the increase in tensile yield stress, and the increase in hardness that were developed for pressure vessel steels.[9-11] The shift in transition temperature, ΔT, with an increase in tensile yield stress, $\Delta\sigma_y$, is expressed as

$$\Delta T\ (°C) = C\Delta\sigma_y\ (MPa), \tag{3}$$

where C ~0.5°C/MPa for plate material, and 0.65°C/MPa for welds. The change in yield stress with hardness, ΔDPH, is given by the relation

$$\Delta\sigma_y\ (MPa) = 3.5\Delta DPH. \tag{4}$$

The shift in the CTT of both LT and TL specimens is 23°C (28°C for LT specimens from inner region) and the increase in yield stress is 51 MPa. The increase in hardness due to irradiation is difficult to obtain because of the variation in hardness across the thickness of the wall. However, annealing studies indicate that the irradiation-induced hardness change, represented by the decrease in hardness after annealing at 400°C for 2 h, is ~4.3 R_B (14 DPH) for locations 3 and 9. This is consistent with Eq. (4). The change in hardness is slightly lower, i.e., ~3.5 R_B (10 DPH), for location 8.

The results from the present study suggest that the unexpectedly high embrittlement of the HFIR surveillance samples may be due to factors other than flux effects. The minor

differences in copper and nickel content between the two materials are not expected to have any effect at the low irradiation temperatures of Shippingport NST and the HFIR. Analytical studies are in progress at ANL to investigate radiation damage measures to determine whether a unified picture of embrittlement in HFIR, ORR, and Shippingport can be achieved. High-flux irradiation experiments will be performed for materials from the Shippingport NST and the HFIR vessel to confirm the analysis and evaluate the possible effects of metallurgical differences between the two materials.

5. Conclusions

Characterization of material from the Shippingport NTS indicates that the embrittlement of A212 grade B steel in a low-temperature, low-flux environment is consistent with that expected from the current NRC regulatory guidelines. The shifts in CTT are between 23 and 28°C (41 and 50°F); the values are not as great as those of the HFIR surveillance samples. The reasons for this difference are not well understood.

The NST weld metal is significantly tougher than the plate material. The weld specimens show a strong affect of location across the thickness of the wall; only the inner regions of the weld show embrittlement. The shift in CTT is ~20°C (36°F).

Acknowledgments

This work was supported by the Office of Nuclear Regulatory Research, U. S. Nuclear Regulatory Commission. The authors are grateful to W. F. Burke and G. M. Dragel for their contributions to the experimental effort and to A. Sather for conducting the mechanical tests.

References

1. R. K. Nanstad, K. Farrel, D. N. Braski, and W. R. Corwin, "Accelerated Neutron Embrittlement of Ferritic Steels at Low Fluence: Flux and Spectrum Effects", J. Nucl. Mater. **158**, 1 (1988).

2. R. D. Cheverton, J. G. Merkle, and R. K. Nanstad, Evaluation of HFIR Pressure Vessel Integrity Considering Radiation Embrittlement, Oak Ridge National Laboratory Report, ORNL/TM-10444 (April 1988).

3. J. R. Hawthorne, "Studies of Radiation Effects and Recovery of Notch Ductility of Pressure Vessel Steels", British Nuclear Energy Conference, Iron and Steel Institute, London, England (1960).

4. S. T. Rosinski, O. K. Chopra, and W. J. Shack, "Shippingport Neutron Shield Tank Sampling and Analysis Program," proceedings of the 1989 ASME Pressure Vessel and

Piping Conference, Honolulu, Hawaii, Eds. D. L. Marriott, T. R. Mager, and W. H. Bamford, Vol. 170, 109 (1989).

5. S. T. Rosinski, W. J. Shack, and O. K. Chopra, "Irradiation Embrittlement Investigation of the Shippingport Station Neutron Shield Tank," to be published in the Proceedings of the Fourth International Symposium on Environmental Degradation of Materials in Nuclear Power Systems - Water Reactors.

6. L. James, Bettis Atomic Power Laboratory, private communication (April 1989).

7. W. L. Server, "Impact Three-Point Bend Testing for Notched and Precracked Specimens", J. Testing and Evaluation **6**, 29 (1978).

8. L. Greenwood, Argonne National Laboratory, unpublished work.

9. G. R. Odette and G. E. Lucas, Irradiation Embrittlement of LWR Pressure Vessel Steels, EPRI Report NP-6114 (January 1989).

10. G. R. Odette and G. E. Lucas, "Irradiation Embrittlement of Reactor Pressure Vessel Steels: Mechanisms, Models and Data Correlation", ASTM-STP-909, American Society for Testing and Materials, Philadelphia, 206 (1986).

11. G. E. Lucas and G. R. Odette, "Recent Advances in Understanding Radiation Hardening and Embrittlement Mechanisms in Pressure Vessel Steels", in *Proc. Second Int. Symp. on Environmental Degradation of Materials in Nuclear Power Systems - Water Reactors*, American Nuclear Society, TMS-AIME-NACE, Monterey, CA, 345 (September 1985).

Table 1. Typical Chemical Composition (wt.%) of the A212 Grade B Plate and Weld Metal from the Shippingport NST

Element	Plate	Weld
C	0.23	0.065
Mn	0.76	0.93
P	0.02	-
S	0.03	-
Si	0.27	0.73[1]
Cu	0.05	0.06[2]
Ni	0.04	0.02
Cr	0.04	0.03
O	0.01	-
N	0.004	-
Ti	<0.005	0.025
V	<0.005	0.019
Zr	<0.005	<0.005
Mo, Ca, Al	<0.01	<0.01
Se, Sn, B	<0.01	<0.01

1 0.86 for inner-wall weld from location 14.

2 0.07 for outer-wall weld and 0.04 for inner-wall weld from location 15

Table 2. Values of the Constants in Eq. (1), Charpy Transition Temperature and Upper Shelf Energy for A212 Grade B Material from the NST Outer and Inner Walls

Sample Location	Sample Region	Orientation	Constants K_0 J/cm²	B J/cm²	C °C	D °C	CTT[1] °C	CTT[1] °F	USE J/cm²	USE ft·lb
				Outer Wall						
All	Inner, Outer	LT	8.6	46.7	33.5	23.2	16	61	102	60
14,15	Center	LT	6.7	48.2	26.0	23.3	9	48	103	61
All	Inner, Outer	TL	8.0	29.3	33.5	30.3	20	68	67	40
14,15	Center	TL	8.0[2]	33.5	18.4	30.3[2]	2	36	74	44
				Inner Wall						
2,8,3,9	Inner	LT	8.3	33.6	53.3	17.2	44	111	76	45
2,8,3,9	Outer	LT	8.2	34.3	47.1	16.1	39	102	77	45
2,8,3,9,14,15	All[3]	TL	4.1	24.1	46.1	25.5	43	109	52	31

1 Charpy transition temperature at 20.3-J level.

2 Values of K_0 and D assumed to be the same as those for inner/outer region.

3 Inner and outer region specimens from locations 2, 8, 3, and 9 and center region specimens from locations 14 and 15.

Table 3. Tensile Properties for A212 Grade B Material from NST Outer and Inner Walls

Sample Region	Test Temperature °C	Outer Wall		Inner Wall	
		Yield Stress MPa	Ultimate Stress MPa	Yield Stress MPa	Ultimate Stress MPa
Inner, Outer	25	305 ± 19	529 ± 10	354 ± 20	554 ± 14
Center	25	268 ± 11	506 ± 23	321 ± 3	522 ± 27
Inner, Outer	55	287 ± 21	508 ± 11	320 ± 15	522 ± 2
Center	55	264 ± 13	476 ± 8	308 ± 4	497 ± 25

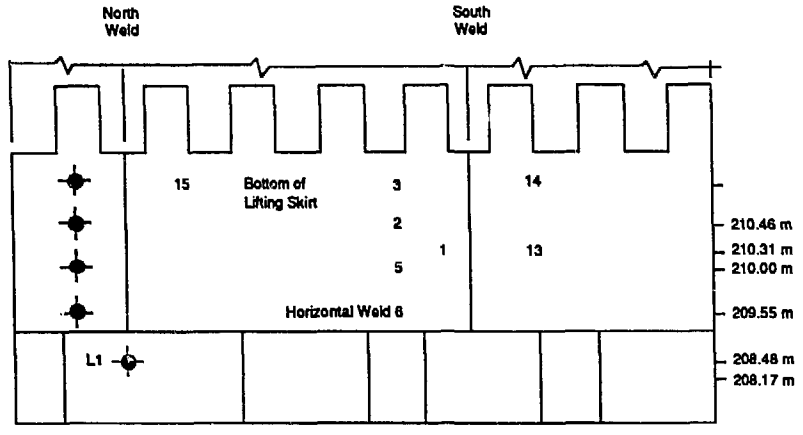

(a)

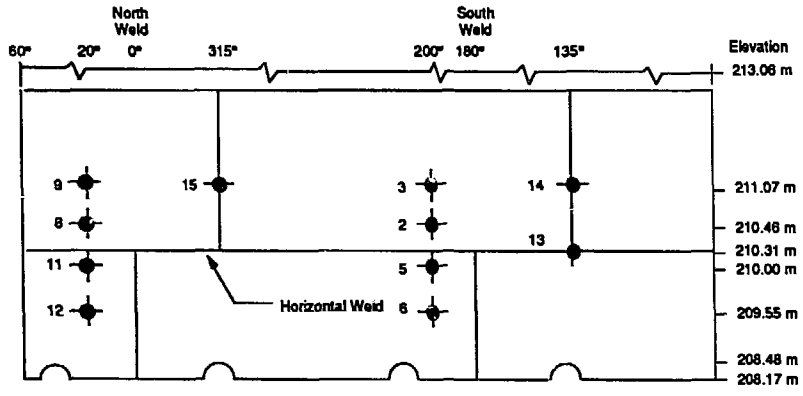

(b)

Figure 1. Layout of Sample Location in the Shippingport NST (a) Outer and (b) Inner Walls.

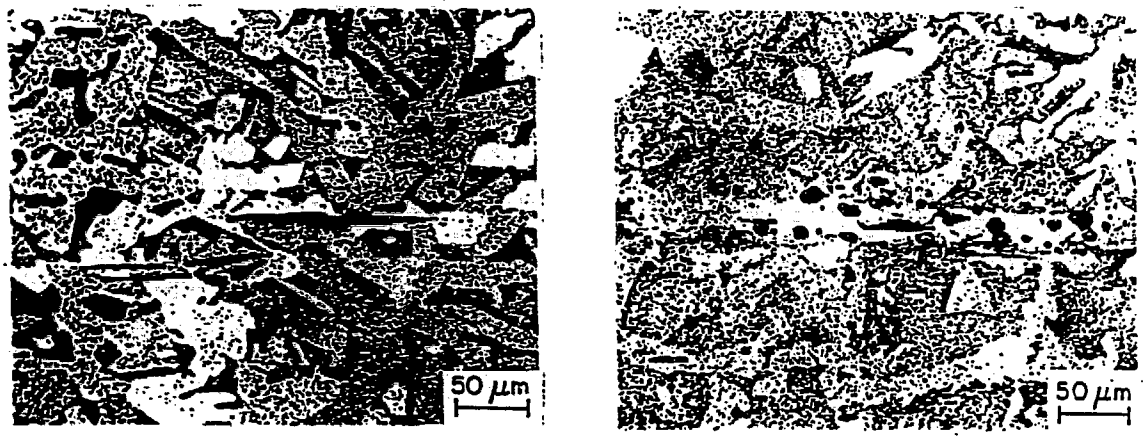

Figure 2. Micrographs of the NST Material Along the (a) Transverse and (b) Rolling Sections.

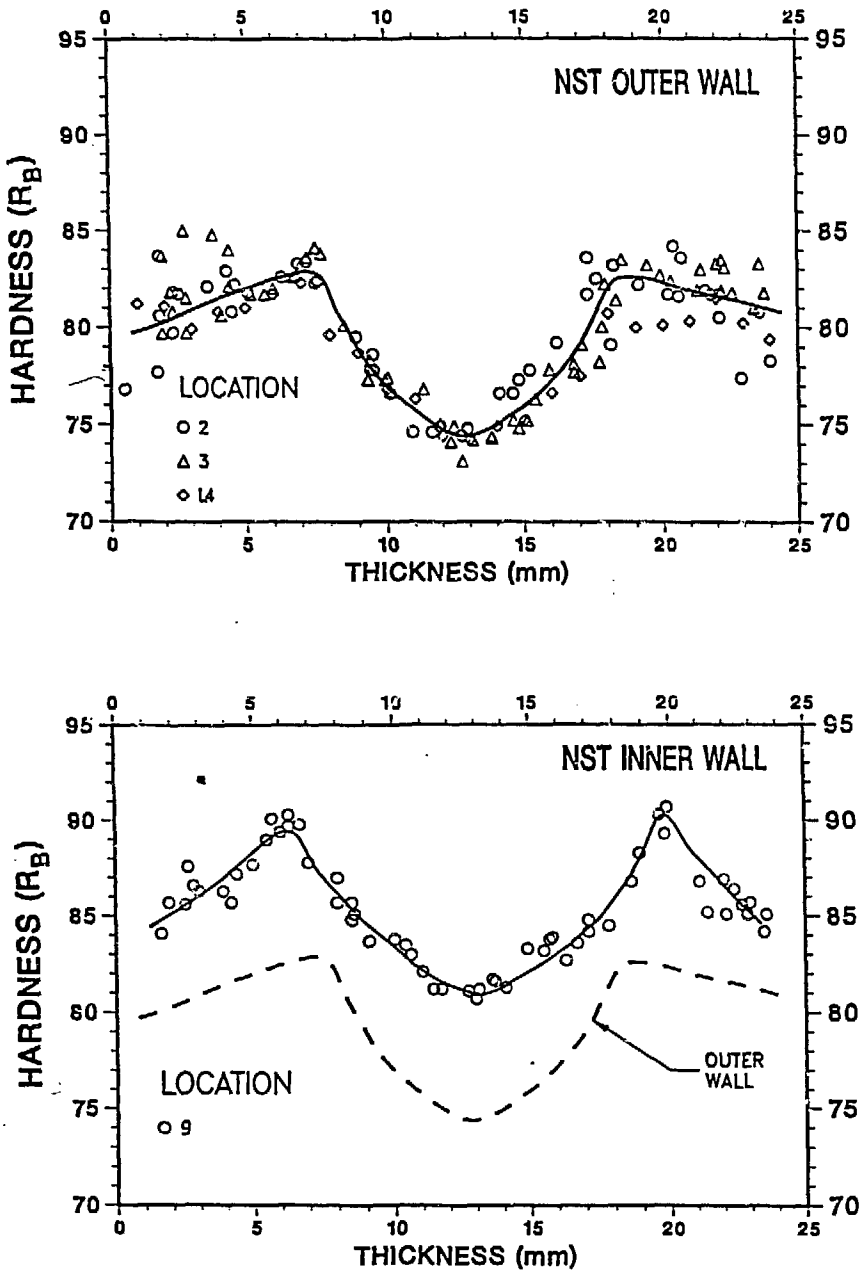

Figure 3. Hardness Profiles across the Thickness of the NST (a) Outer and (b) Inner Wall.

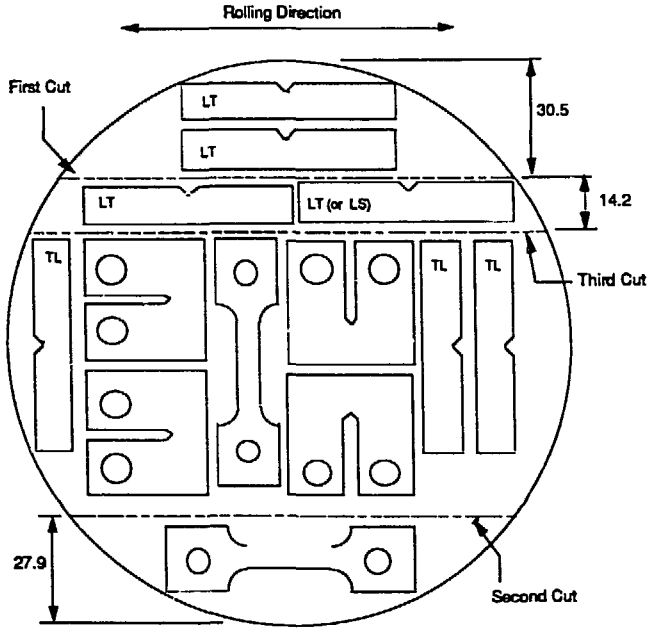

Note: Diagram based on an assumed diameter of 146 mm
All Dimensions in mm.

Figure 4. Cutting Diagram for Base Metal Samples from the NST Inner and Outer Walls.

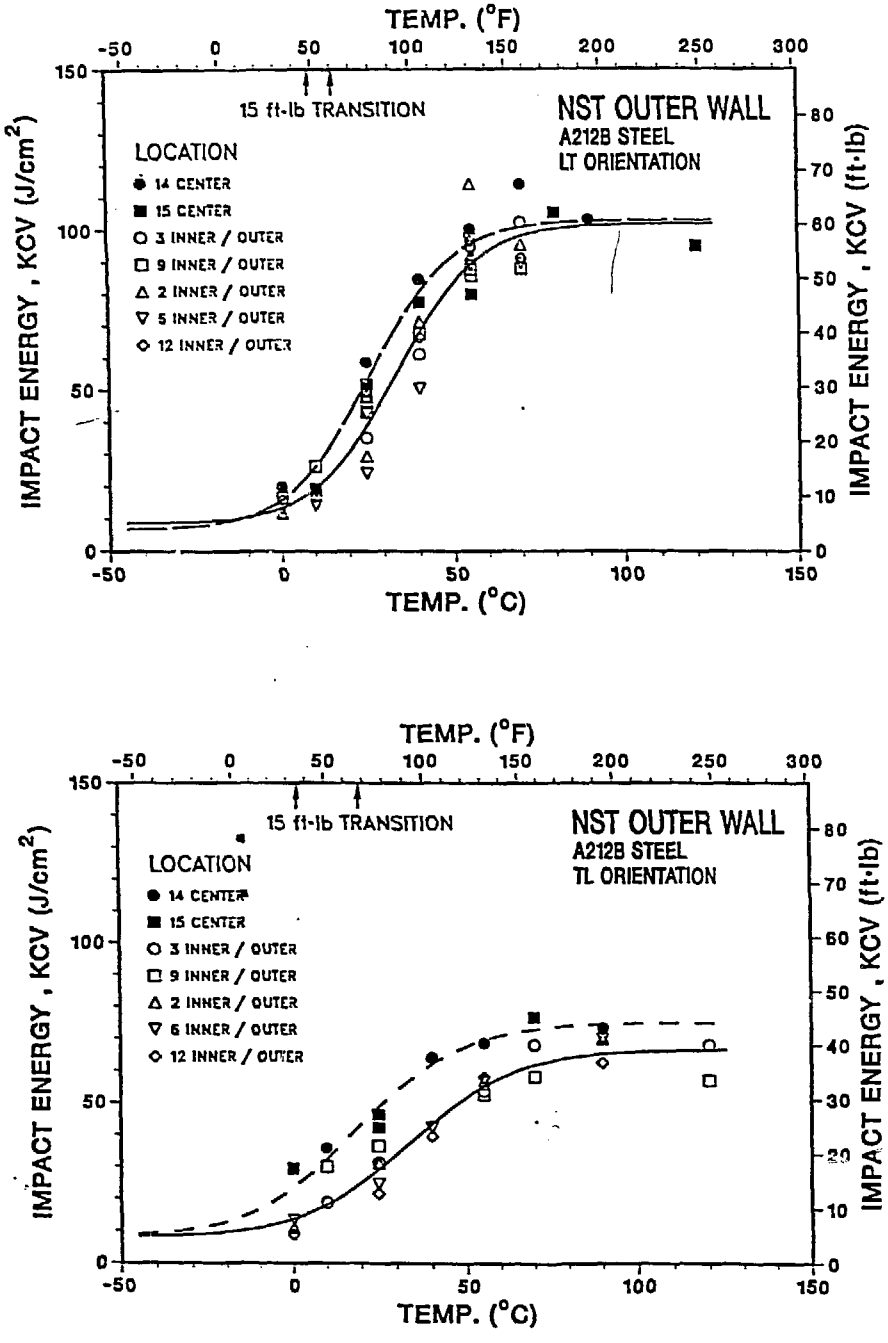

Figure 5. Charpy Impact Test Data for (a) LT and (b) TL Specimens for the NST Outer Wall.

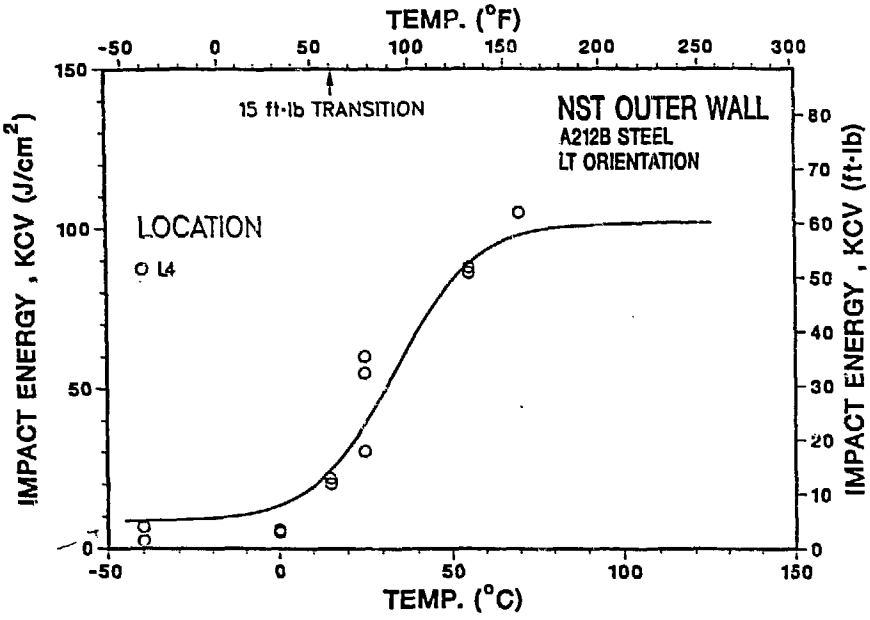

Figure 6. Charpy Impact Test Data for LT Specimens from Location L4 of the NST Outer Wall.

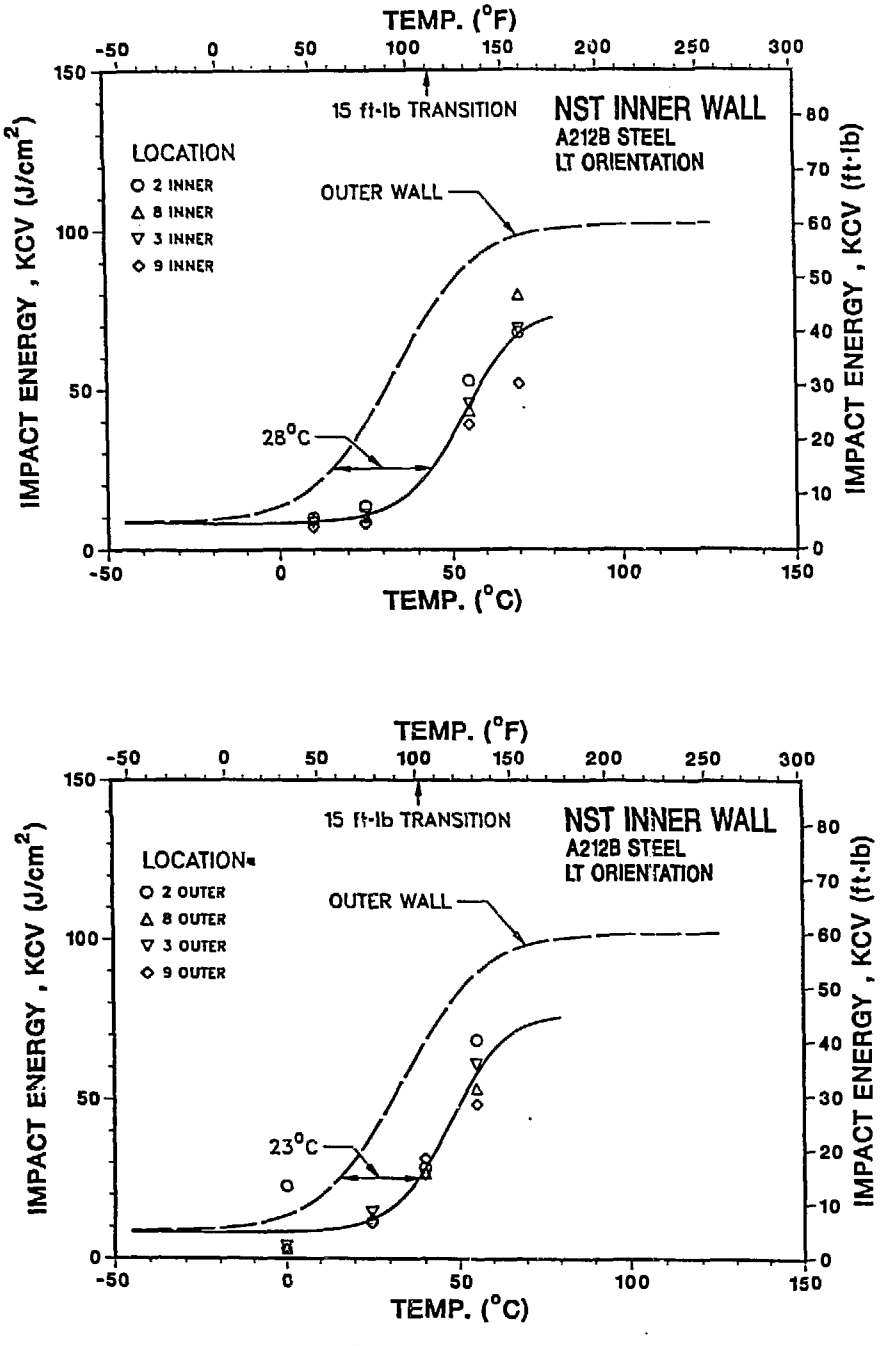

Figure 7. Charpy Impact Test Data for (a) and (b) LT and (c) TL Specimens for the NST Inner Wall.

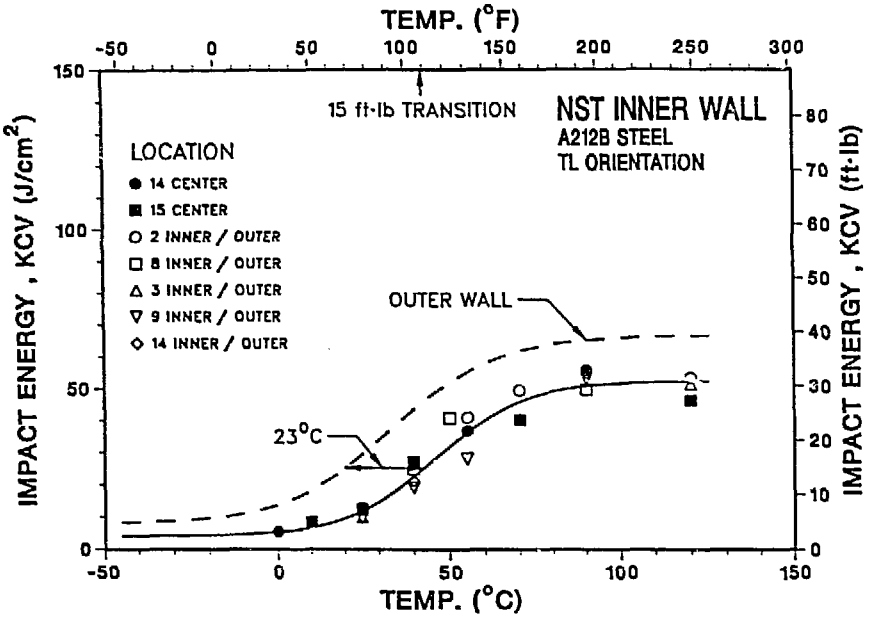

Figure 7. (Contd.)

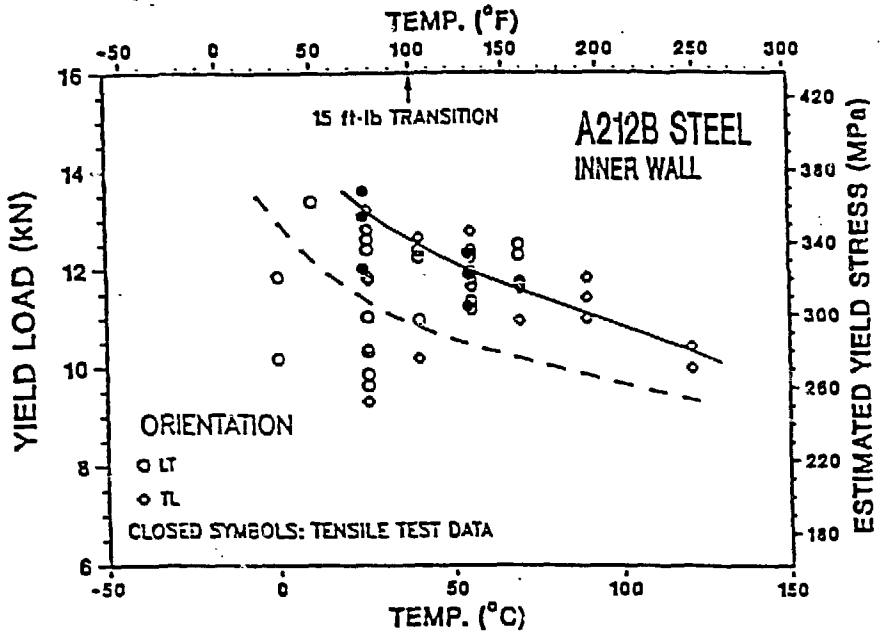

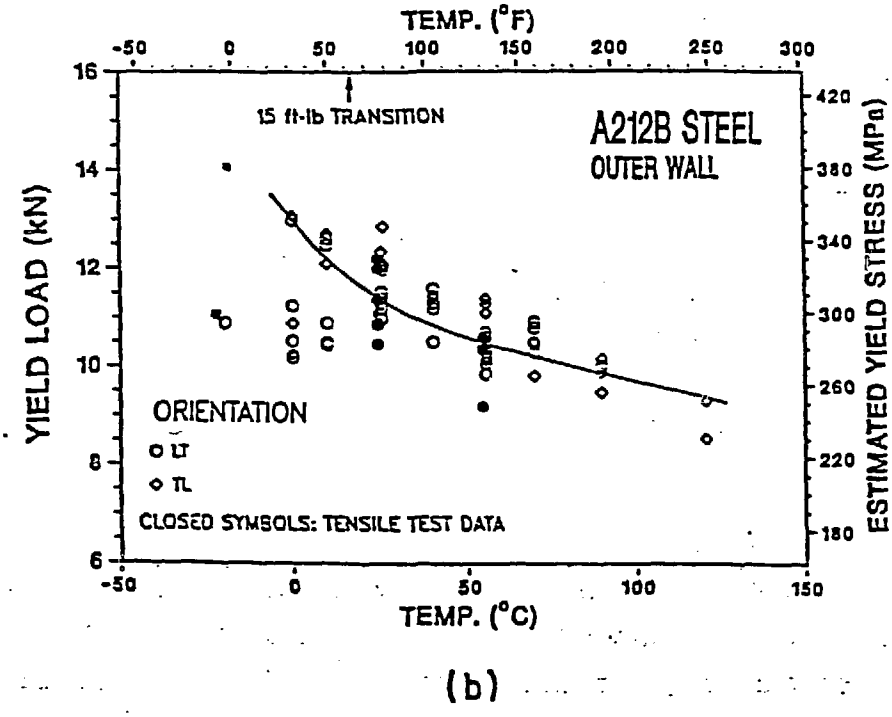

Figure 8. Yield and Ultimate Stress Estimated from the Charpy Impact Data for the NST (a) Outer and (b) Inner Walls.

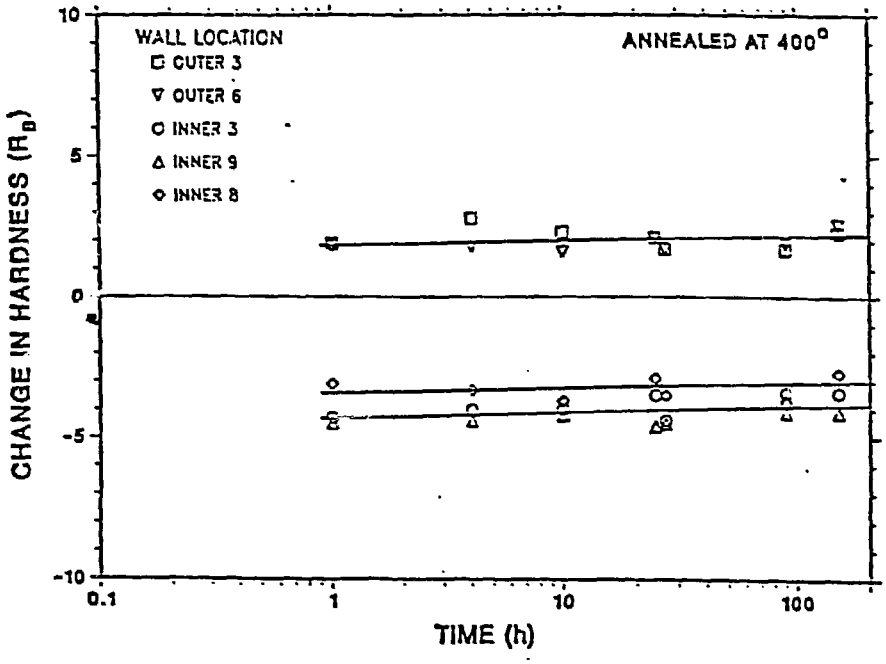

Figure 9. Change in Hardness of the Neutron Shield Material from Inner and Outer Walls after Annealing at 400°C.

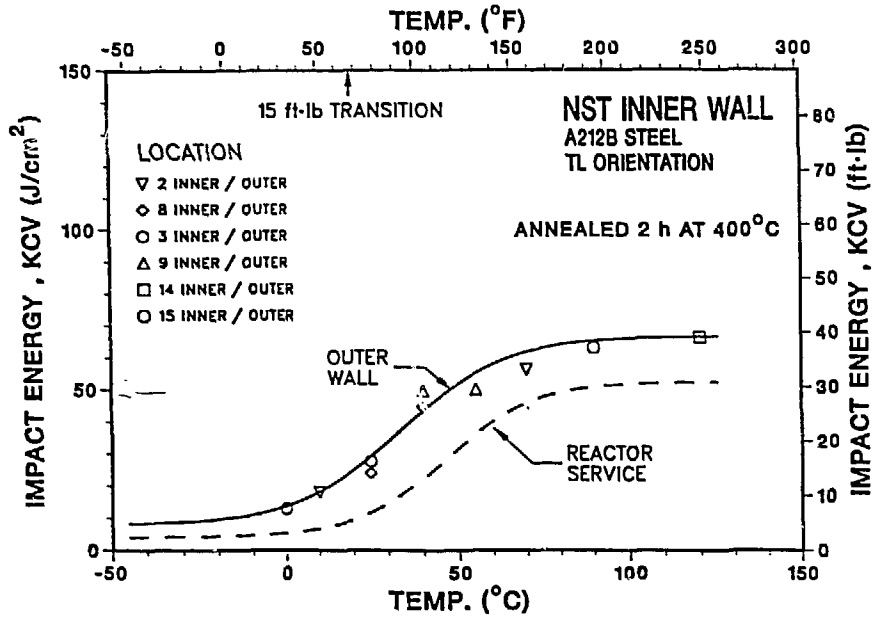

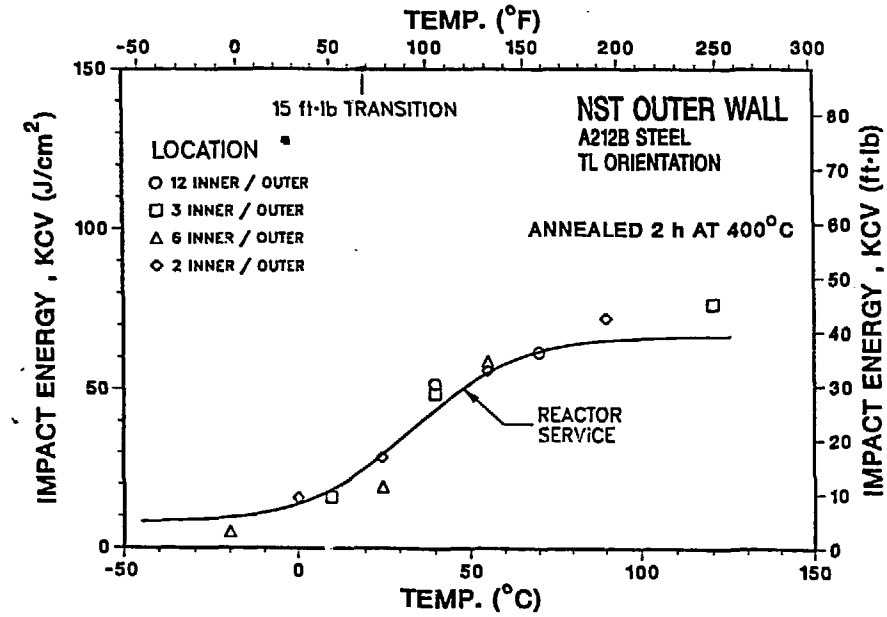

Figure 10. Charpy Impact Test Data for Annealed TL Specimens from (a) Inner Wall and (b) Outer Wall.

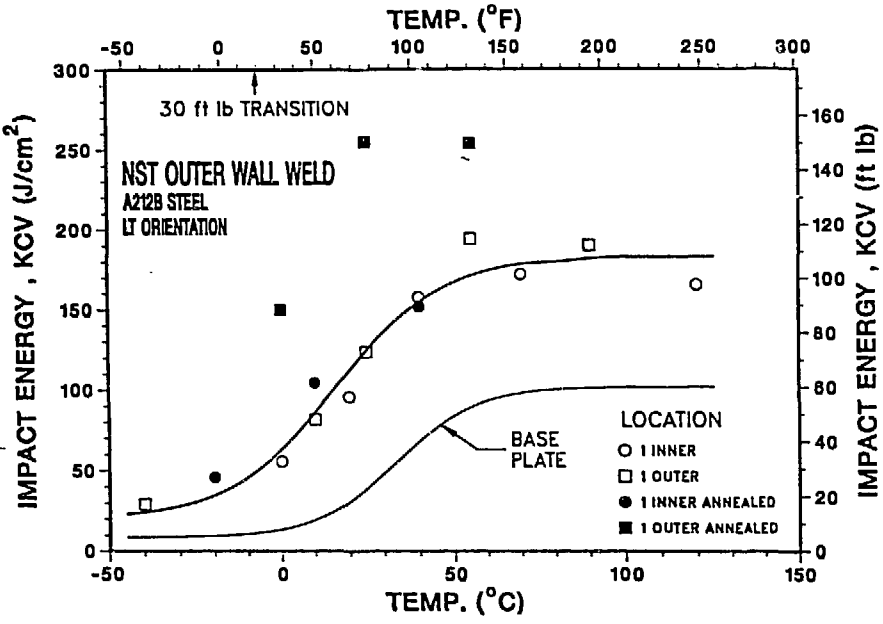

Figure 11. Charpy Impact Test Data for Weld Metal Specimens from NST Outer Wall.

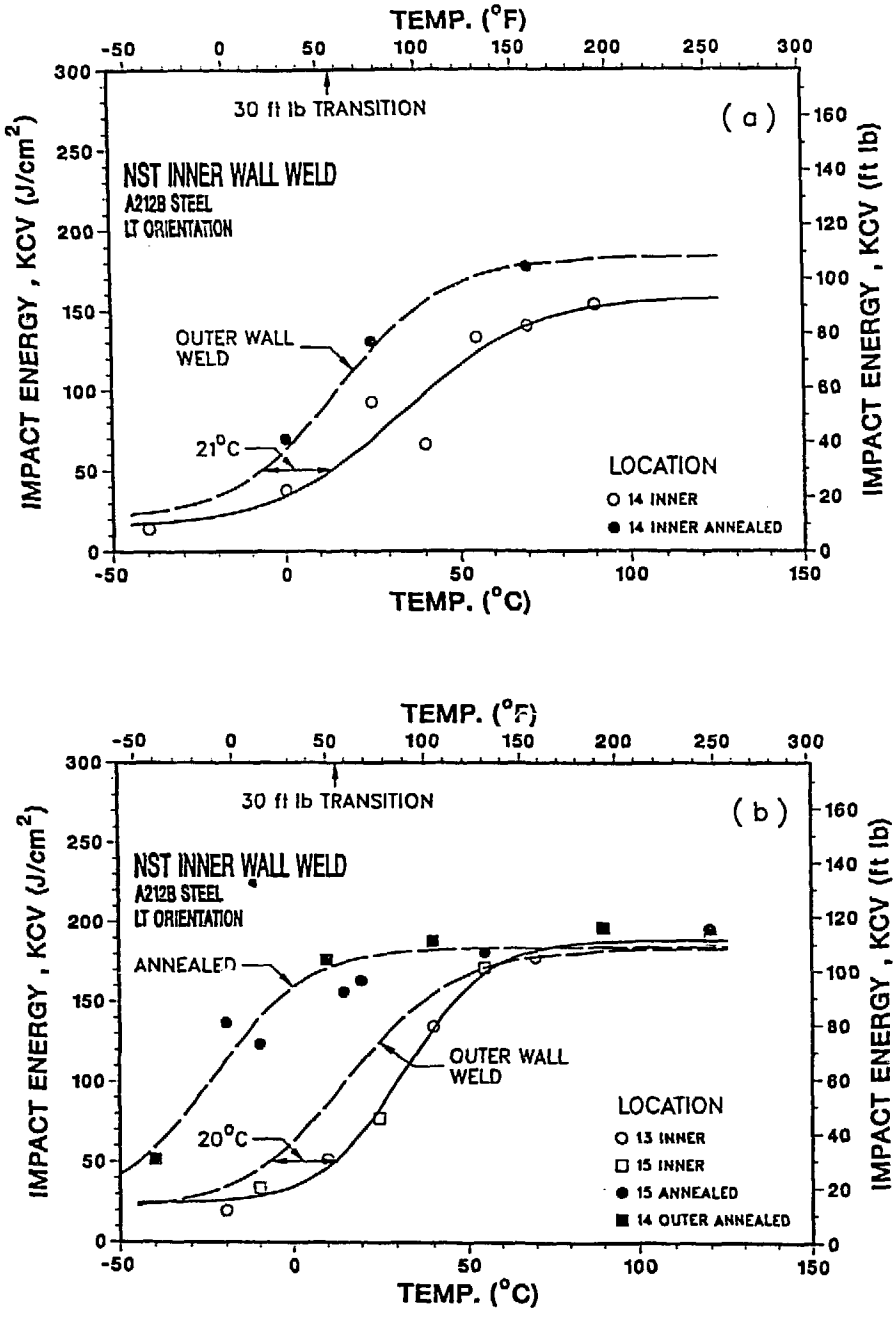

Figure 12. Charpy Impact Test Data for Weld Metal Specimens from (a) and (b) Inner Region and (c) and (d) Outer Region of NST Inner Wall.

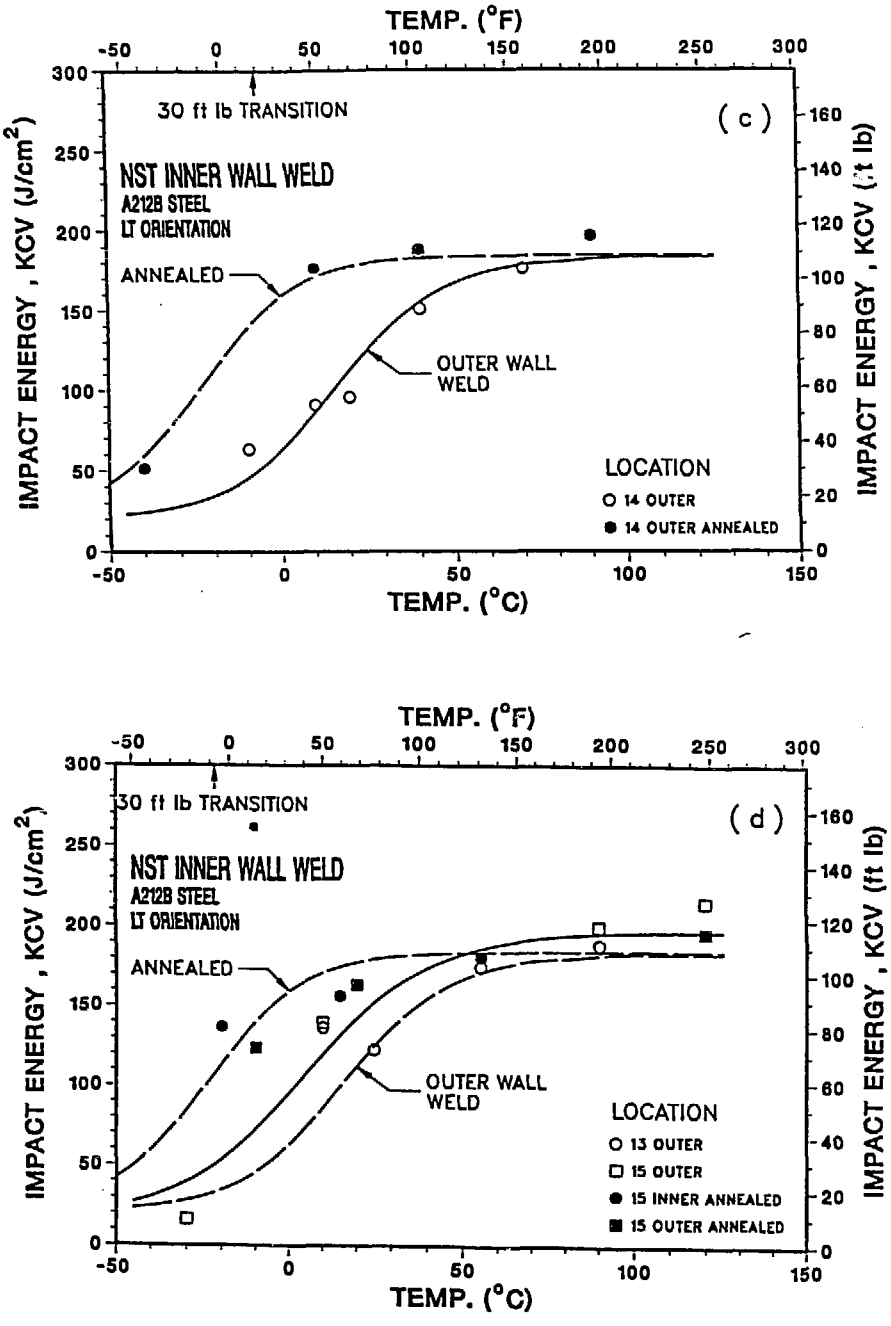

Figure 12. (Contd.)

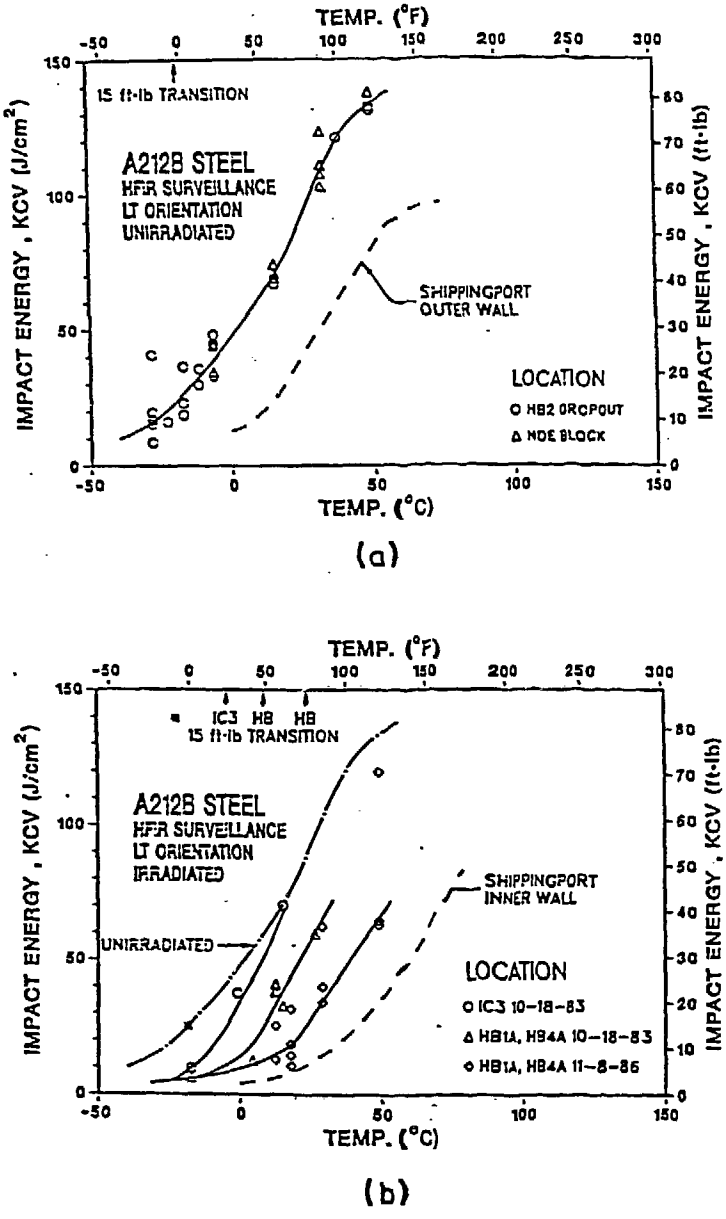

Figure 13. Comparison of Charpy Impact Data for (a) Unirradiated and (b) Irradiated Shippingport NST and HFIR Surveillance Samples.

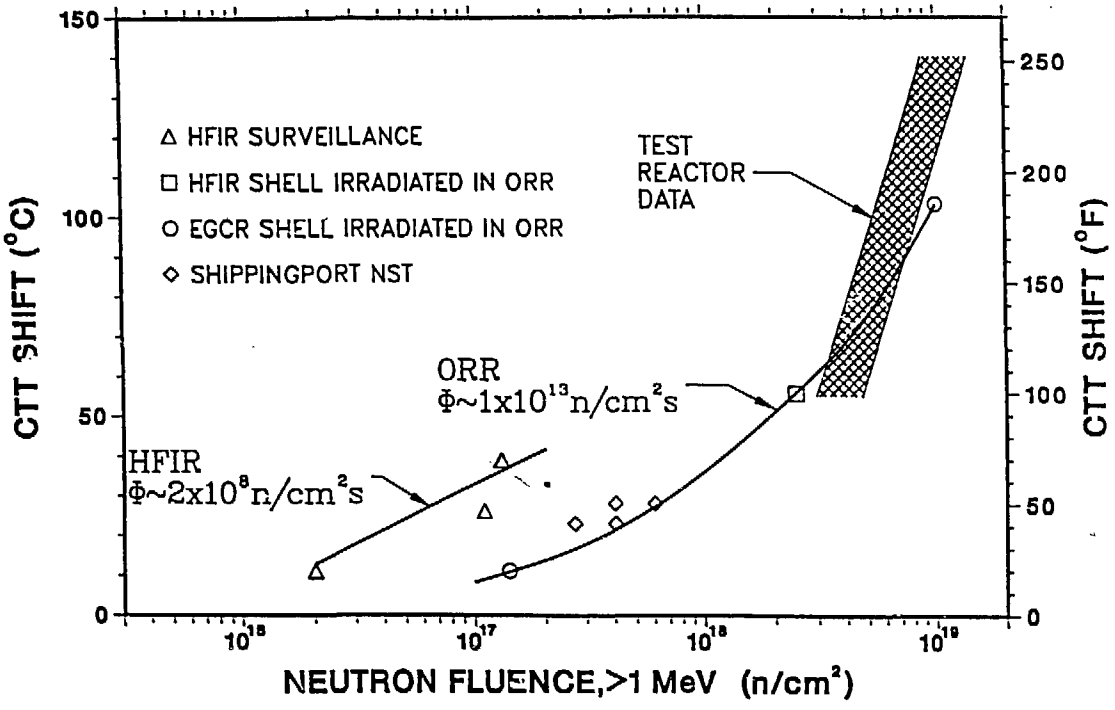

Figure 14. Comparison of Transition Temperature Shifts for Shippingport NST with HFIR Surveillance Results and A212B data from High-Flux Test Reactors.